International Journal of Fluid Machinery and Systems
Vol. 3, No. 1, January-March 2010

Original Paper

Surrogate Modeling for Optimization of a Centrifugal Compressor Impeller

Jin-Hyuk Kim[1], Jae-Ho Choi[2] and Kwang-Yong Kim[1]

[1]Department of Mechanical Engineering, Inha University
253 Yonghyun-Dong, Incheon, 402-751, Republic of Korea
jinhyuk@inha.edu, kykim@inha.ac.kr
[2]Power Systems R&D Center, Samsung Techwin
28 Sungju-Dong, Changwon-City, Gyeonsangnam-do, 641-717, Republic of Korea
jaeho1.choi@samsung.com

Abstract

This paper presents a procedure for the design optimization of a centrifugal compressor. The centrifugal compressor consists of a centrifugal impeller, vaneless diffuser and volute. And, optimization techniques based on the radial basis neural network method are used to optimize the impeller of a centrifugal compressor. The Latin-hypercube sampling of design-of-experiments is used to generate the thirty design points within design spaces. Three-dimensional Reynolds-averaged Navier-Stokes equations with the shear stress transport turbulence model are discretized by using finite volume approximations and solved on hexahedral grids to evaluate the objective function of the total-to-total pressure ratio. Four variables defining the impeller hub and shroud contours are selected as design variables in this optimization. The results of optimization show that the total-to-total pressure ratio of the optimized shape at the design flow coefficient is enhanced by 2.46% and the total-to-total pressure ratios at the off-design points are also improved significantly by the design optimization.

Keywords: Centrifugal compressor, Impeller, Meridian plane, Optimization, Pressure ratio, Efficiency.

1. Introduction

Numerical optimization methods based on the surrogate model combined with three-dimensional Reynolds-averaged Navier-Stokes equations (RANS) have been widely applied for the internal flow analysis due to a three-dimensional and vortical flow structure in the rotating passage of turbomachinery [1, 2]. Especially, application of these numerical optimization methods has reduced the computational cost and time to predict the optimal design of a centrifugal compressor to enhance the performance parameters.

Design optimization coupled with a CFD (computational fluid dynamics) code was performed for a centrifugal compressor by Bonaiuti and Pediroda [3]. Bonaiuti et al. [4] reported the optimization of transonic centrifugal compressor impellers using a design-of-experiments technique. They selected meridional contour and angle of the impellers as design variables. Wang et al. [5] performed aerodynamic optimization design of a centrifugal compressor impeller with the Kriging model. Bartold and Joos [6] carried out optimization of a centrifugal impeller using evolutionary algorithms with three-dimensional RANS solver.

The pressure ratio of centrifugal compressors is important especially for applications in turbochargers and industrial gas turbines. Benini [7] achieved to maximize the pressure ratio and efficiency of a transonic compressor rotor by defining the blade profile with Bezier curve parameters for the multi-objective optimization. The total pressure ratio and efficiency considered to enhance the performance of a compressor blade was used as an objective variable to optimize a compressor blade based on three-dimensional RANS analysis by Samad and Kim [8]. Merchant et al. [9] described the experimental investigation of an aspirated fan stage and the design using an axisymmetric through-flow code coupled with a quasi three-dimensional cascade plane code in order to achieve a pressure ratio of 3.4:1 at 1500feet/sec. Wu et al. [10] used the total pressure ratio, mass flow and efficiency as an objective function and showed that pressure ratio and rotor loading can be improved further through optimizing swirl distribution using adaptive simulated annealing (ASA) algorithm. Merchant et al. [11] demonstrated the possibility of substantially increasing the pressure ratio of a compressor stage at a given tip speed and increased the pressure ratio by controlling the development of blade and end-wall boundary layer in region of adverse pressure gradient by means of boundary layer suction.

Received September 20 2009; accepted for publication December 21 2009: Review conducted by Dr. Tadashi Tanuma. (Paper number O09044)
Corresponding author: Kwang-Yong Kim, Professor, kykim@inha.ac.kr

Optimization techniques based on the radial basis neural network (RBNN) method have been applied for the design of turbomachinery by many researchers. Cosentino et al. [12] used a genetic algorithm coupled with an artificial neural network method to optimize a three-dimensional impeller described by 15 geometrical parameters. The RBNN method based optimization procedure has been applied by Huppertz et al. [13]. The RBNN method coupled with the response surface of a low-order polynomial has been reported for turbomachinery design by Rai and Madyavan [14]. Lee et al. [15] applied optimization of an axial flow fan blade for efficiency enhancement using the RBNN techniques. Samad et al. [16] compared different surrogate along with the RBNN to optimize compressor blade shape.

In this work, a numerical optimization using the RBNN method coupled with three-dimensional RANS analysis has been performed for the design of a centrifugal compressor impeller. The meridian flow path has been optimized by four design variables out of the control points, wherein Bezier curves are used to construct the curves of the shroud and the hub. The objectives of this work are to enhance the total-to-total pressure ratio of the impeller by means of the proposed design method and to examine the differences in the flow field between the reference and the optimum impellers to gain understanding of the flow physics associated with the improved the pressure ratio.

2. Numerical Analysis

The flow analysis is performed through a finite volume solver. Blade profile creation, computational mesh generation, boundary-condition definitions, flow analysis and post processing are performed through Blade-Gen, Turbo-Grid, CFX-Pre, CFX-Solver, and CFX-Post, respectively [17].

The meridian view of the centrifugal compressor is shown in Fig. 1. The impeller inlet and outlet planes are located at *Stations 1* and *2*, respectively. The diffuser outlet plane is located at *Station 3*. The flow parameters, such as the total pressure and total temperature, etc., in relation to the mass flow rates are measured at the stations. The inlet boundary of the computational domain is located 65mm upstream from the impeller leading edge and the exit boundary is located 80mm downstream from the diffuser exit. The specifications of the reference centrifugal compressor are summarized in Table 1. Here, the blade angle is defined as the radial direction.

As shown in Fig. 2, the total pressure and total temperature at the inlet are set to 1.0 atm and 298.0K, respectively. The air is considered as an ideal gas and the designed mass flow rate is set at the outlet for steady-state simulation. The solid surfaces are considered to be hydraulically smooth with no-slip and adiabatic conditions. Periodic conditions are set at the blade passage interfaces and tip clearance is modeled as 0.5mm.

The shear stress transport (SST) turbulence model [18] is used as the turbulence closure. The SST model uses a k-ω model at the near-wall region and a k-ε model in the bulk domain; a blending function ensures a smooth transition between the two models, viz., k-ω and k-ε.

A structured grid system is constructed in the computational domain, which has O-type grids near the blade surfaces and H/J/C/L-type grids in the other regions. The inlet and outlet blocks are constructed using 30,000 and 80,000 grid points, respectively, while the main passage is constructed using 150,000 grid points. The grid dependency test is performed and the results are shown in Fig. 3 for the velocity of spanwise location at the trailing edge. Thus, a total of 260,000 nodes are used to define a passage with a splitter. Fig. 4 shows an example of the grid system.

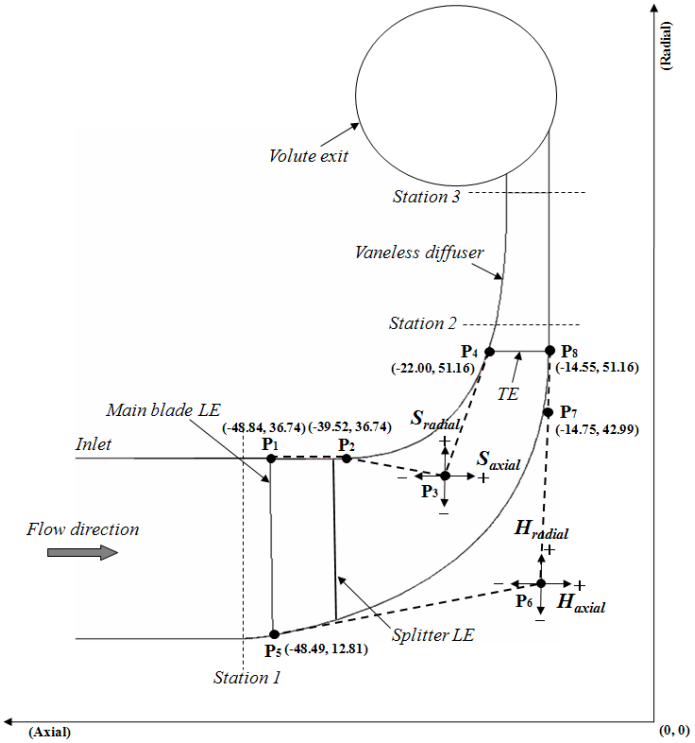

Fig. 1 Meridian view of the centrifugal compressor

Table 1 Design specifications and constraints of the centrifugal impeller

Flow coefficient	0.14
Rotational speed, rpm	65,550
Total pressure ratio	1.96
Impeller outlet diameter, mm	102.32
Number of blade (splitter)	6 (6)
Inlet blade angle (hub, tip), degree	-54.12, -62.96
Outlet blade angle (hub, tip) , degree	-28.98, -32.14

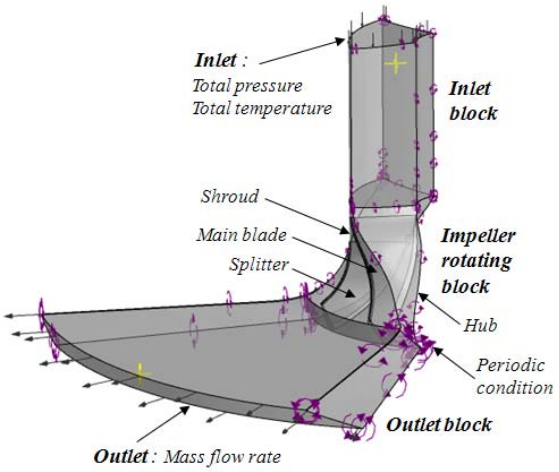

Fig. 2 Computational domain and boundary conditions

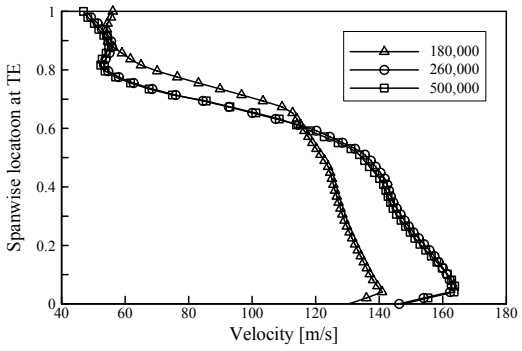

Fig. 3 The results of the grid dependency test

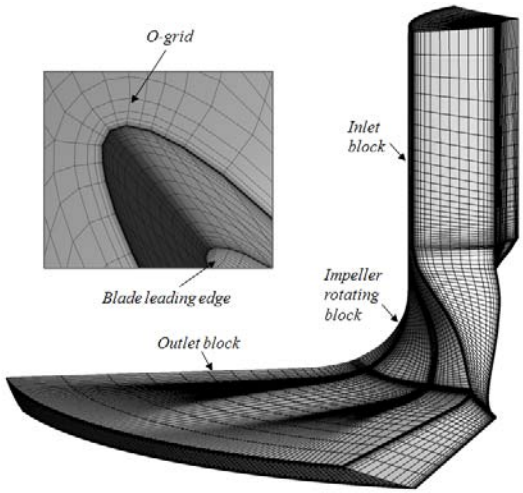

Fig. 4 Structure of the grid system

The root mean squared (RMS) residual values of the momentum and mass were set to fall below 1.0E-06 and the imbalances of mass and energy were kept below 1.0E-03 as part of the convergence criteria. The physical time-scale is set to 0.1/ω, where ω is the angular velocity of the blades. The converged solutions are obtained after approximately 500 iterations. The computations have been performed by a PC with an Intel Pentium IV CPU and a clock speed of 3.0 GHz. The computational time is about 5-6 hours depending upon the geometry considered and the rate of convergence.

3. The Objective Function and Design Variables

The purpose of the current optimization problem is to maximize the total-to-total pressure ratio (PR), which is defined as:

$$PR = \frac{P_{t,st2}}{P_{t,st1}} \tag{1}$$

where, P_t is total pressure, and the subscripts, st1 and st2, respectively, indicate *Station 1* and *Station 2* of the centrifugal compressor as shown in Fig.1.

The geometric parameters related to the shroud and hub contours of the impeller are selected as the design variables. The three-dimensional contours cannot be handled in a conventional compressor design even though they seem very sensitive to the pressure ratio. It is necessary to optimize the three-dimensional impeller shape since the flow structures in the impeller passage are three-dimensional in nature. Thus, the meridian contours are selected for changing the impeller shape among many geometric variables. The meridian contours affect the curvature of the shroud and hub contours, blade height, and the passage and annulus areas along the meridian path for a fixed blade angle and thickness.

As shown in Fig. 1, each meridian contour at the hub or shroud can be changed by moving one of the four control points that are used to construct curves in the form of third-order Bezier curves. The variations of P_3 and P_6 along the axial and radial directions are selected as the design variables. The leading and trailing edges of the impeller are fixed in this optimization. And, P_2 and P_7 are also fixed in order to obtain a smooth slope at the impeller inlet tip and the impeller exit hub. Therefore, S_{radial}, S_{axial}, H_{radial} and H_{axial} are used for the design variables in this study.

The main advantage of the parameterization of contours by Bezier curves is that some limited number of points (called the 'control points') can control the curves. The curves are smooth and free from discontinuities. A Bezier curve of order, n, is defined by Bernstein polynomials as follows:

$$C(t) = \sum_{i=0}^{n} B_{i,n}(t) P_i \tag{2}$$

In Eq. (2), the Bezier blending function is as follows:

$$B_{i,n}(t) = \binom{n}{i} t^i (1-t)^{n-1} \tag{3}$$

$$\text{If } P_i = (x_i, y_i), \text{ then } x(t) = \sum_{i=0}^{n} x_i B_{i,n}(t)$$

$$\text{and } y(t) = \sum_{i=0}^{n} y_i B_{i,n}(t),$$

where t is the parameter of the curve that is normalized over [0 1] and $\{P_i\}$ are the coordinates of the control points. In the present study, the curve is defined by a third-order polynomial.

4. Optimization Techniques

In the present work, the RBNN method is used to obtain the optimal shape of a centrifugal compressor impeller. The RBNN model is constructed based on the evaluations of the objective function at the prescribed design points through training. The main advantage of using the radial basis approach is the ability to reduce the computational cost due to the linear nature of the radial basis functions. RBNN uses a linear combination of N radially symmetric functions, $g_i(x)$, for the response function as [19]:

$$F(x_i) = \sum_{i=1}^{N} w_i g_i(x) + \varepsilon_i \tag{4}$$

where, w_i are the coefficients of the linear combination, g_i are the radial basis functions, and ε_i is the set of errors with equal variance, σ^2.

RBNN method is a two-layered network with a hidden layer of radial basis transfer function with linear output. The hidden layer consists of a set of radial basis functions that act as activation functions. The design parameters for this function are a spread constant (SC) and a user-defined error goal (EG). The SC value is selected such that it should not be so large that each neuron does not respond in the same manner for all the inputs and it should not be so small that the network becomes highly sensitive for every input within the design space.

EG (or mean square error goal selection) is also important. A small error goal will produce over-training of the network, while a large error goal will affect the accuracy of the model. In the present work, we used a customized the RBNN function *newrb* available in MATLAB [20]. The leave-one-out cross validation (also known as PRESS in polynomial response surface approximation terminology) [16] has been performed to assess the accuracy of the models. Although, it is uncertain that how well the cross-validation correlates with the model accuracy, it is nearly unbiased estimation of generalization errors as it takes into account the cross-validation of the surrogate at every design point.

The optimization procedure is shown in Fig. 5. Four variables are initially selected and the design space is decided. The design points within design space are selected with the help of Latin-hypercube sampling (LHS) as the design of experiment (DOE) [21]. LHS, an effective sampling method in DACE, is a matrix $m \times n$ order, where m is the number of levels (sampling points) to be examined and n is the number of design variables. Each of the n columns of the matrix containing the levels 1,2, …, m is randomly paired to form a LHS. It generates random sample points, ensuring that all portions of the design space are represented. Therefore, LHS of design of experiments is used to generate thirty design points within design spaces in this work.

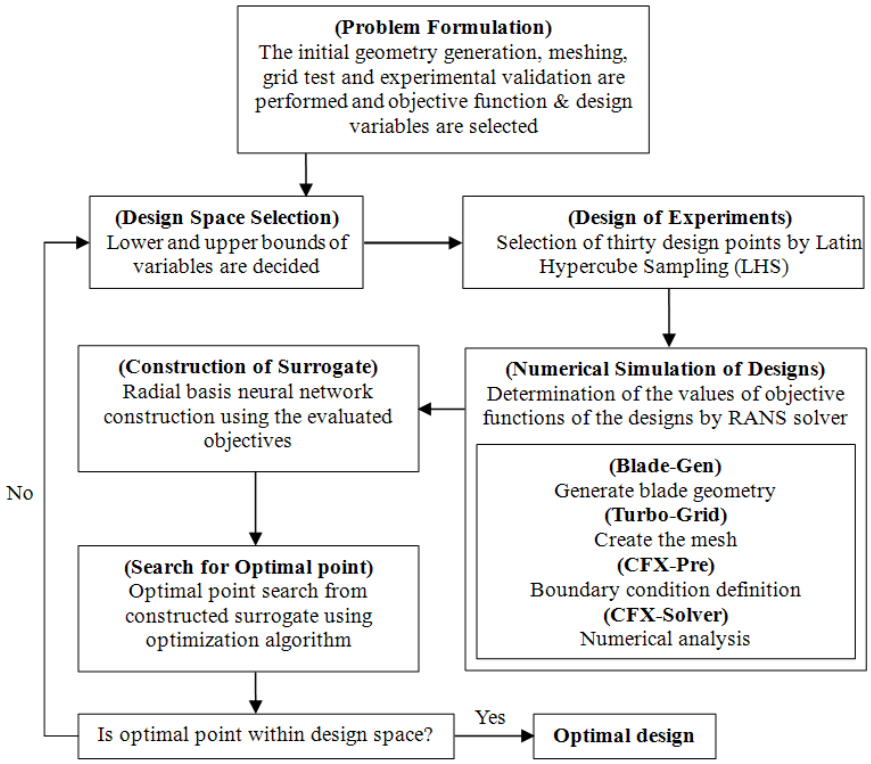

Fig. 5 Optimization procedure

The evaluations of the objective functions at these design points are carried out by solving three-dimensional RANS equations. The values of the design variables at these design points and the corresponding objective functions are used to train the network. The neural network model is constructed by RBNN, and the optimum point is searched by Sequential Quadratic Programming (SQP) [20].

5. Results and Discussion

The numerical results for the flow analysis have been validated prior to design optimization. A compressor performance test was performed at the test rig shown in Fig. 6. The shape of the impeller and the diffuser used for this test are regarded as the reference shapes, that is, the initial shapes for the present optimization. Further, the numerical results are validated through a comparison with the test data for these reference shapes. The compressor inlet is defined as the impeller inlet (*Station 1*) and the outlet is defined as the volute outlet (*Station 4*). Fig. 7 shows the validation of the results of flow analysis in comparison with the results of the test of performance with regard to the total pressure ratio and the isentropic efficiency. The pressure ratios and efficiencies are in good agreements with the test data at low flow coefficients but some discrepancies are present at high flow coefficients.

For design optimization, it is important to find the feasible and practical design space that is formed by setting up the ranges of the design variables. Thirty design points are determined by Latin-hypercube sampling technique in this design space. Objective function values at design points are evaluated by RANS analyses, and the results are used to train the RBNN model. The ranges of the design variables are presented in Table 2. The variables are normalized by the impeller exit radius.

The accuracy of the RBNN model is checked by varying EG and SC in order to obtain the minimum PRESS (Prediction Error Sum of Squares) for training data. In the RBNN model, SC value, EG and PRESS were set as 0.45, 2.51×10^{-4} and 2.39×10^{-2}, respectively. The PRESS is an estimate of the average square error over the entire domain.

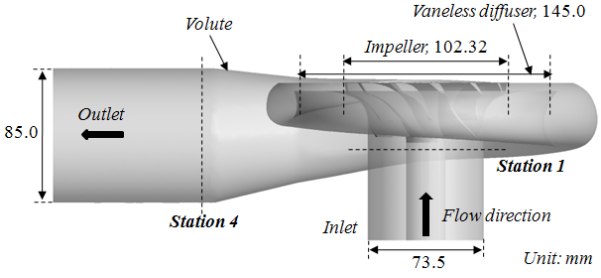

Fig. 6 Measurement stations of the centrifugal compressor

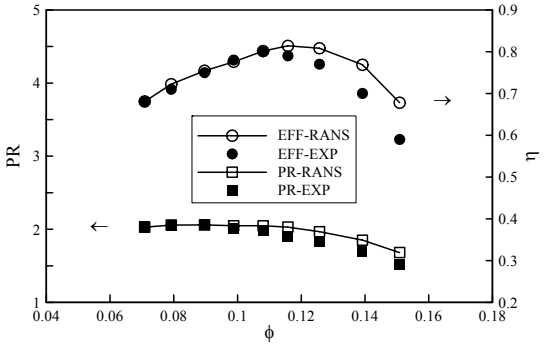

Fig. 7 Validation of the flow analysis

The optimum design variables for the present compressor impeller are found by the RBNN method and listed in Table 3, and the shape is shown in Fig. 8. The shroud contour is optimized to have larger curvatures along the whole meridian path. But, the hub contour is optimized to have smaller curvatures. It is noticed that the curvature at the shroud is relaxed after optimization. Fig. 9 shows the passage areas of the reference and the optimum impeller along the meridian length. The areas are normalized by the inlet passage area of the impeller. The optimum impeller has the passage area larger than that of the reference impeller along the entire meridian length. Especially, it has much larger area in the range of 25~85% meridian length.

The PR of the compressor at the design flow coefficient for the reference impeller is calculated as 1.965 as shown in Table 4. The PR of the optimum impeller is estimated to be 2.019 by RBNN method at the optimum design variables, and calculated as 2.014 by RANS analysis. The RBNN method gives a good prediction for the optimum efficiency in comparison with the value calculated by RANS analysis. And, the PR is enhanced by 2.43% with the present optimization at the design flow coefficient.

In order to compare PR performances at off-design conditions, flow analyses are performed at several flow coefficients for the reference and the optimum impellers, and performance of the reference impeller with the increased rotation speed, 66,618 rpm is also presented. With the optimization, nearly uniform improvement in the PR is observed throughout the entire range of the flow coefficient from near-surge to near-choke region in Fig. 10. Therefore, it is found that the off-design performance is also enhanced by the present design optimization. It is also seen that the PR of the reference impeller at the increased rotation speed becomes nearly same as that of the optimum impeller near the design flow coefficient. Therefore, the optimum impeller produces as high PR with the rotation speed (65,550 rpm) of the reference as the increased rotation speed (66,618 rpm).

Table 2 Ranges of the design variables

Variables	S_{radial}	S_{axial}	H_{radial}	H_{axial}
Lower	0.666	-0.554	0.370	-0.420
Reference	0.666	-0.534	0.385	-0.302
Upper	0.686	-0.495	0.542	-0.288

Table 3 Optimum design variables

Design	Design variables			
	S_{radial}	S_{axial}	H_{radial}	H_{axial}
Reference	0.666	-0.534	0.385	-0.302
PR	0.685	-0.551	0.371	-0.289

Table 4 Results of the optimization

Design	Prediction	CFD calculation		Increment (%)	
	Objective	PR	η	PR	η
Reference	-	1.965	0.860	-	-
PR	2.019	**2.014**	0.864	**2.43**	0.46

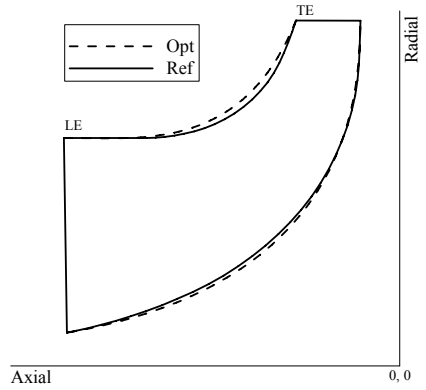

Fig. 8 Comparison of the blade profiles at the meridian plane

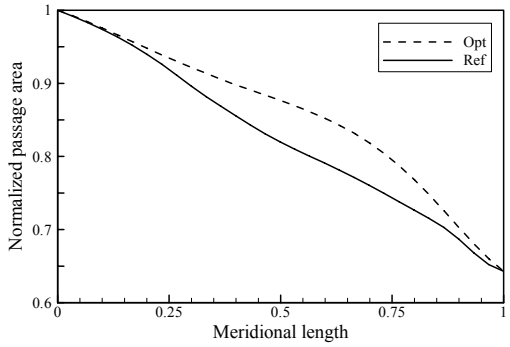

Fig. 9 Comparison of passage areas along the meridian length

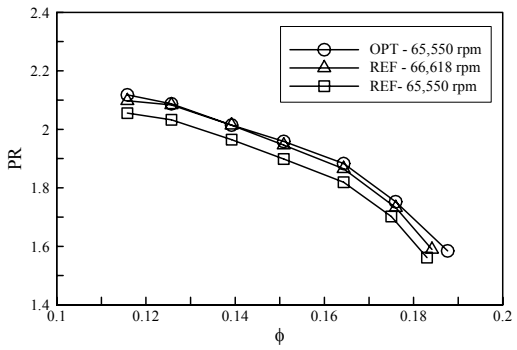

Fig. 10 Comparison of the total-to-total pressure ratio curves

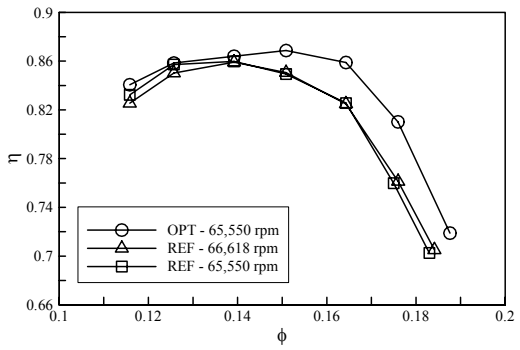

Fig. 11 Comparison of the isentropic efficiency curves

Total-to-total isentropic efficiency is also an important performance specification for compressor. So, the isentropic efficiencies achieved by the optimum and the reference impellers, respectively, are compared with that of the reference impeller with the increased rotation speed at the design and off-design points in Fig. 11. At the design point, the efficiency of the optimum impeller is improved by 0.49% in comparison with the reference impeller, and entirely has higher value in a wide range from near-surge point to near-choke point. Especially, remarkable improvement in the efficiency is found in the range of higher flow coefficient, and the rotating speed of the reference impeller does not affect the efficiency unlike the case of PR shown in Fig. 10.

The total pressure contours on the meridian plane at low flow (ϕ=0.12), design (ϕ=0.14) and high flow (ϕ=0.16) coefficients are shown in Figs. 12, 13 and 14, respectively. In these figures, the differences among the contours in two reference and the optimum impellers are found mainly near the trailing edge. The optimum impeller of each flow coefficient has the highest pressure near the hub of the impeller trailing edge. The increased passage area of the optimum impeller shown in Fig. 9 yields the higher pressure. The static pressure characteristics at two spanwise locations (20% and 80% span) of the reference and the optimum impellers are shown in Figs. 15 and 16. The static pressure contours in the optimum and the reference impellers show similar distribution at 20% span (Fig. 15), but remarkable differences are found at 80% span (Fig. 16). The static pressure becomes more uniform in the optimum impeller in blade-to-blade direction on the suction surface of the splitter near the trailing edge at 80% span.

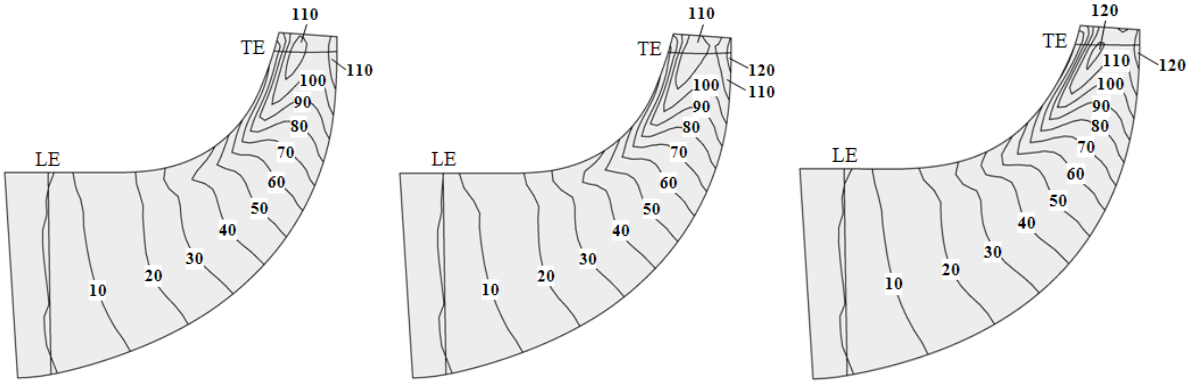

(a) Reference (b) Reference (66,618rpm) (c) Optimum

Fig. 12 Total pressure distributions on the meridian plane at ϕ=0.12 (unit: kPa)

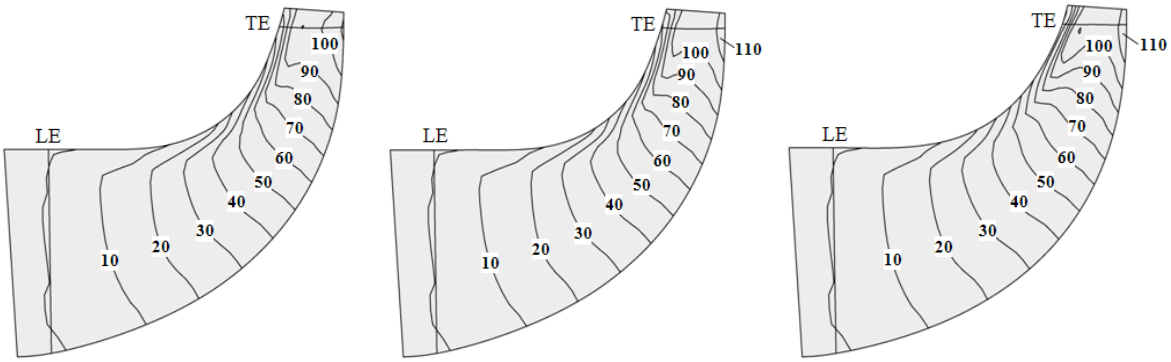

(a) Reference (b) Reference (66,618rpm) (c) Optimum

Fig. 13 Total pressure distributions on the meridian plane at ϕ=0.14 (unit: kPa)

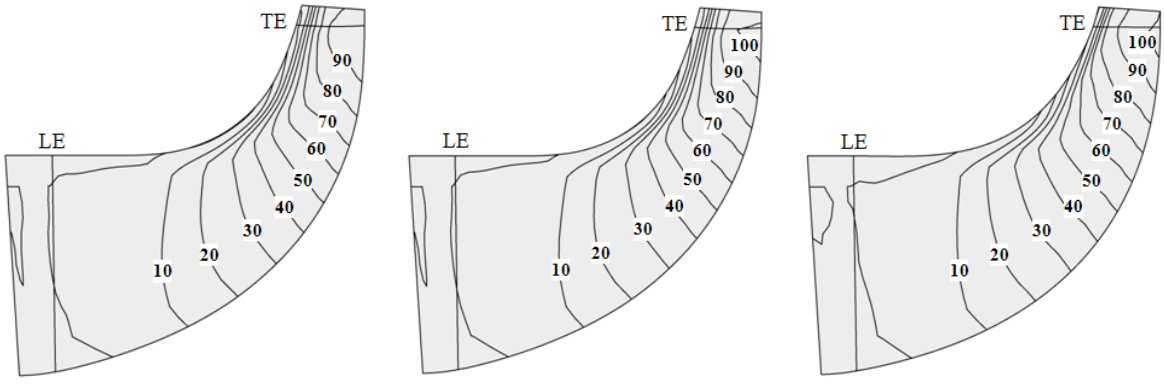

(a) Reference (b) Reference (66,618rpm) (c) Optimum

Fig. 14 Total pressure distributions on the meridian plane at ϕ=0.16 (unit: kPa)

Fig. 17 shows the static pressure contours on the blade suction surfaces of the reference and the optimum impellers. A low pressure zone caused by the flow separation near the blade leading edge is observed in the reference impeller. However, it is relaxed in the optimum blade. Because the flow passage area is increased on the meridian plane of the optimum impeller as shown in Figs. 8 and 9, the pressure gradient near leading edge of the optimum blade becomes lower, and this reduces the separation zone.

The Static pressure distributions and contours at the trailing edge are shown in Figs. 18 and 19, respectively. Averaged static pressures at each span are shown in Fig. 18, which shows nearly uniform increment of pressure by the optimization throughout the whole spanwise locations. And, Fig. 19 shows the static pressure contours at the trailing edge. The optimum impeller shows lower static pressure at the shroud of the suction surface, and higher value at the hub of the pressure surface in comparison with the reference impeller.

6. Conclusion

An optimization of a centrifugal compressor impeller has been performed by the RBNN method through three-dimensional RANS analyses to enhance total-to-total pressure ratio. In order to optimize the meridian flow path, four design variables are selected from two control points for constructing the shroud and hub contours. Validation of the numerical results is performed through experimental data for the pressure ratios and efficiencies. The results of the optimization show that the pressure ratio of the optimum impeller at the design flow coefficient is enhanced by 2.43% in comparison with the reference impeller, and the pressure ratios at the off-design flow coefficients are also improved similarly. The total pressure ratio has been improved through the optimized passage area along the meridian length. The results show that the present optimization method with RANS analysis can be an efficient tool for the design optimization of a centrifugal compressor impeller in light of the pressure ratio.

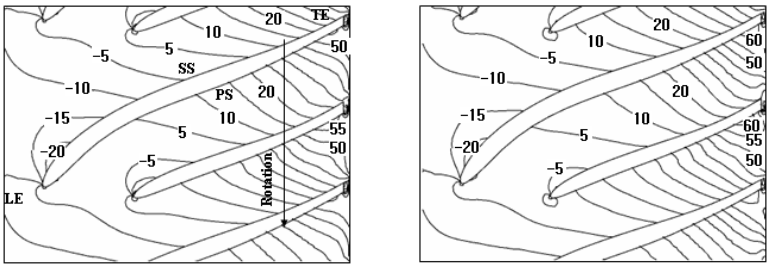

(a) Reference (b) Optimum

Fig. 15 Static pressure contours at a span of 20%

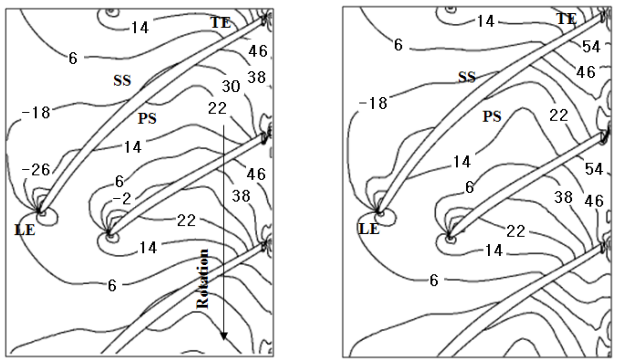

(a) Reference (b) Optimum

Fig. 16 Static pressure contours at a span of 80%

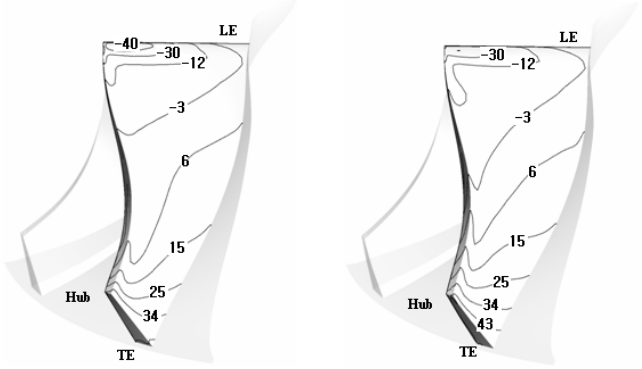

(a) Reference (b) Optimum

Fig. 17 Static pressure contours on the suction surface of the blade

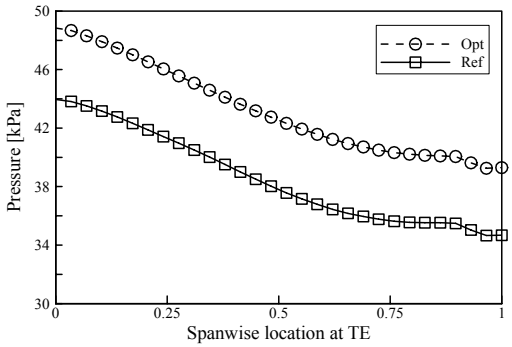

Fig. 18 Static pressure distributions at the trailing edge

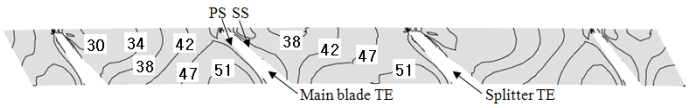

(a) Reference

(b) Optimum

Fig. 19 Static pressure contours at the trailing edge

Acknowledgments

This research was supported by a grant (No. 10031771) from the Korea Institute of Industrial Technology Evaluation and Planning (ITEP) that is funded by the Ministry of Knowledge Economy.

Nomenclature

H_{axial}	Design variable for axial variation of control point at hub	S_{axial}	Design variable for axial variation of control point at shroud
H_{radial}	Design variable for radial variation of control point at hub	S_{radial}	Design variable for radial variation of control point at shroud
k	Ratio of the specific heat	SS	Suction surface
LE	Leading edge	TE	Trailing edge
P	Static pressure	η	Isentropic efficiency ($\eta = \{(P_{t,out}/P_{t,in})^{k-1/k}\}/\{(T_{t,out}/T_{t,in})-1\}$)
P_i	Coordinates of control points		
PS	Pressure surface	ϕ	Flow coefficient
Subscript			
in	Inlet	out	Outlet

References

[1] Jang, C. M., and Kim, K. Y., 2005, "Optimization of a Stator Blade Using Response Surface Method in a Single- Stage Transonic Axial Compressor," Proceedings of the Institution of Mechanical Engineers, Part A, Journal of Power and Energy, Vol. 219, No. 8, pp. 595-603.

[2] Nakamura, K., and Kurosawa, 2009, "Design Optimization of a High Specific Speed Francis Turbine Using Multi-Objective Genetic Algorithm," International Journal of Fluid Machinery and Systems, Vol. 2, No. 2, pp. 102-109.

[3] Bonaiuti, D., and Pediroda, V., 2001, "Aerodynamic Optimization of an Industrial Centrifugal Compressor Impeller Using Genetic Algorithms," Proceedings of Eurogen 2001.

[4] Bonaiuti, D., Arnone, A., Ermini, M., 2006, "Analysis and Optimization of Transonic Centrifugal Compressor Impellers Using the Design of Experiments Technique," Journal of Turbomachinery, Vol. 128, October, pp. 786-797.

[5] Wang, X. F., Xi, G., and Wang, Z. H., 2006. "Aerodynamic Optimization Design of Centrifugal Compressor's Impeller with Kriging Model," Proceedings of the Institution of Mechanical Engineers, Part A, Journal of Power and Energy, Vol. 220, No. 6, pp. 589-597.

[6] Bartold, A., and Joos, F., 2008, "Optimization of a Centrifugal Impeller using Evolutionary Algorithms," ASME Turbo Expo 2008, Berlin, Germany, GT2008-50805.

[7] Benini, E., 2004, "Three-Dimensional Multi-Objective Design Optimization of a Transonic Compressor Rotor," Journal of Propulsion and Power, Vol. 20, No. 3, pp. 559-565.

[8] Samad, A., and Kim, K. Y., 2009, "Application of Surrogate Modeling to Design of A Compressor Blade to Optimize Stacking and Thickness," International Journal of Fluid Machinery and Systems, Vol. 2, No. 1, pp. 1-12.
[9] Merchant, A., Kerrebrock, J. L., Adamczyk, J. J., and Braunscheidel, E., 2004, "Experimental Investigation of a High Pressure Ratio Aspirated Fan Stage," ASME Turbo Expo 2004, Vienna, Austria, GT2004-53679.
[10] Wu, H., Li, Q., and Zhou, S., 2007, "Optimization of Highly Loaded Fan Rotor Based on Through Flow Model," ASME Turbo Expo 2007, Montreal, Canade, GT2007-27603.
[11] Merchant, A. A., Drela, M., Kerrebrock, J. L., Adamczyk, J. J., and Celestina, M., 2000, "Aerodynamic Design and Analysis of a High Pressure Ratio Aspirated Compressor Stage," ASME Turbo Expo 2000, Munich, Germany, 2000-GT-619.
[12] Cosentino, R., Alsalihi, Z., and Van den Braembussche, R., A., "Expert System for Radial Impeller Optimization," Proc., Fourth European Conference on Turbomachinery, Paper No. ATI-CST-039/01.
[13] Huppertz, A., Flassig, P. M., Flassig, R. J., and Swoboda, M., 2007, "Knowledge-Based 2D Blade Design Using Multi-Objective Aerodynamic Optimization and a Neural Network," ASME Turbo Expo 2007, Montreal, Canada, GT2007-28204.
[14] Rai, M. M. and Madyavan, N. K., 2000, "Aerodynamic Design Using Neural Networks," AIAA Journal, Vol. 38, No. 1, pp. 173-182.
[15] Lee, K. S., Kim, K. Y., Samad, A., and Jung, S. H., 2008, "Optimization of an Axial Flow Fan Blade for Efficiency Enhancement Using Neural Network Techniques," The 2nd International Symposium on Jet Propulsion and Power Engineering," Guilin, China, 2008-ISJPPE-4011.
[16] Samad, A., Kim, K. Y., Goel, T., Haftka, R. T., and Shyy, W., 2008, "Multiple Surrogate Modeling for Axial Compressor Blade Shape Optimization," Journal of Propulsion and Power, Vol. 24, No. 2, pp. 302-310.
[17] ANSYS CFX-11.0 Solver Theory, 2006, Ansys Inc.
[18] Menter, F. R., Kuntz, M., and Langtry, R., 2003, "Ten Years of Industrial Experience with the SST Turbulence Model," Turbulence, Heat and Mass Transfer, Begell House Inc.
[19] Orr., M. J. L., 1996, "Introduction to radial basis neural network," Center for cognitive science, Edinburgh University, Scotland, UK. http://anc.ed.ac.uk/RBNN/.
[20] MATLAB®, The Language of Technical Computing, Release 14, 2004, The Math Works Inc.
[21] JMP® 5.1, 2004, SAS Institute, Inc.